$Ni_2M^{II}Te^{IV}{}_2O_2(PO_4)_2(OH)_4$ (M^{II} = Ni, Zn): Synthesis, Crystal Structure, and Magnetic Properties①

CHEN Jia-Ze[a] ZHUANG Rong-Chuan[b]
MI Jin-Xiao[a] HUANG Ya-Xi[a②]

[a] (*Fujian Key Laboratory of Advanced Materials* (*Xiamen University*), *Department of Materials Science and Engineering, College of Materials, Xiamen University, Xiamen* 361005, *China*)

[b] (*State Key Laboratory of Comprehensive Utilization of Low-grade Refractory Gold Ores, Shanghang* 364200, *China*)

ABSTRACT Two isostructural tellurite phosphates $Ni_2M^{II}Te^{IV}{}_2O_2(PO_4)_2(OH)_4$ (M^{II} = Ni, Zn) have been synthesized via hydrothermal method. Both of them crystalize in monoclinic space group *C*2/*m* (No. 12). For $Ni_2ZnTe^{IV}{}_2O_2(PO_4)_2(OH)_4$, a = 19.3247(10), b = 5.9697(3), c = 4.7737(2) Å, β = 103.637(5)°, V = 535.18(5) Å^3, Z = 2, M_r = 727.94, S = 1.103, D_c = 4.517 g·cm^{-3}, μ(Mo$K\alpha$) = 11.434 mm^{-1} and F(000) = 672, the final R = 0.0369 and wR = 0.1086 for 639 observed reflections with $I > 2\sigma(I)$. The crystal structure of $Ni_2M^{II}Te^{IV}{}_2O_2(PO_4)_2(OH)_4$ (M^{II} = Ni, Zn) features a 3*D* framework composed of $[Ni_2O_2(PO_4)_2]^{6-}$ layers interconnected by $[MTe_2O_2(OH)_4]^{2+}$ single chains. Different magnetic susceptibility results at low temperature of the two title compounds confirm that Zn(1) completely occupies the Ni(2) position but not partially substitutes both Ni(1) and Ni(2) position atoms. Additionally, the acentric $TeO_3(OH)_2$ tetragonal pyramids are aligned in an antiparallel manner, resulting in the crystallization of centrosymmetric (*C*2/*m*) crystal structure instead of the non-centrosymmetric crystal structure. The investigation of the origin of centrosymmetric crystal structure with strong dipole moment units provides deeper understanding for future rational design for non-centrosymmetric crystal structure.

Keywords: tellurite, phosphate, crystal structure, stereo-chemically active lone pair, centrosymmetric;
DOI: 10.14102/j.cnki.0254-5861.2011-3194

1 INTRODUCTION

The non-centrosymmetric (NCS) crystal structure compounds have attracted much attention due to their special physical properties, such as piezoelectricity, ferroelectricity, and second-order nonlinear optical (NLO) behavior[1-4]. Great efforts have been made to design and explore NCS crystal structures. One effective strategy is to introduce asymmetric structural units intentionally into the crystal structure, such as the use of cations (Pb^{2+}, Bi^{3+}, Te^{4+}) with stereo-chemically active lone pair (SCALP), the d^0 transition metal cations (Ti^{4+}, Mo^{6+}, W^{6+}) and d^{10} transition metal cations (Zn^{2+}, Cd^{2+}) with strong polar displacements[4-8]. As a result, various NCS crystal structure compounds have been designed and synthesized with wide applications[9-12].

Te^{4+} ion contains stereo-chemically active lone pair (SCALP). It can not only form asymmetric units with second-order Jahn-Teller (SOJT) distortion[4, 13, 14], but can also form various structural building units TeO_x (x = 3, 4 or 5) polyhedra[4, 15-17]. The combination of these TeO_x polyhedra with perfect binding group PO_4 can effectively give compounds with abundant structure types, which could be a very promising direction to search for non-centrosymmetric crystal structure. Up to date, dozens of tellurite phosphates or telluro-phosphates with rich structure chemistry[2, 5, 7, 18-27] have been reported, for example, such as the 1*D* chain compound $Ba_2TeO(PO_4)_2$[19], the 2*D* layer compounds $Te_2O_3HPO_4$[25], $NaTePO_5$[27], $K_2TeP_2O_8$[12], $Ba_2Cu_2Te_2P_2O_{13}$[26] and $SrTeP_2O_8$[27], and the 3*D* framework compounds $Na_3Ca_4(TeO_3)(PO_4)_3$[24], $Ba_2Zn_2TeP_2O_{11}$[22], $Te_2O(PO_4)_2$[7] and $Co_3Te_2O_2(PO_4)_2(OH)_4$[21]. Recently, our group have also reported a tellurite phosphate β-$Te_3O_3(PO_4)_2$[16], which is

Received 26 March 2021; accepted 7 June 2021 (**CCDC 2072715 for $Ni_2ZnTeIV_2O_2(PO_4)_2(OH)_4$**)

① Supported by the National Natural Science Foundation of China (No. 21201144) and the Natural Science Foundation of Fujian Province (No. 2018J07006)

② Corresponding author. E-mail: yaxihuang@xmu.edu.cn

polymorphic with α-$Te_3O_3(PO_4)_2$[18]. In our processive study on tellurite phosphate, we attempt to add d^{10} transition metal Zn with polar displacements into TeO_2-P_2O_5 system to deepen the understanding on the essential factors controlling the formation of non-centrosymmetric crystal structure. As a result, a new nickel zinc tellurite phosphate $Ni_2ZnTe^{IV}{}_2O_2(PO_4)_2(OH)_4$ (designated as NiZnTePO) and an unitary nickel tellurite phosphate $Ni_3Te^{IV}{}_2O_2(PO_4)_2(OH)_4$ (designated as NiTePO) have been observed, while the zinc tellurite phosphate has not been obtained successfully. Here we report the synthesis, crystal structure, and characterizations of two tellurite phosphates, and the discussion of the origin of centrosymmetric crystal structure.

2 EXPERIMENTAL

2. 1 Synthesis

The single crystals of $Ni_2ZnTe^{IV}{}_2O_2(PO_4)_2(OH)_4$ were synthesized via a modified hydrothermal method. A mixture of $NiCl_2$ $6H_2O$ (0.238 g, 1.0 mmol), $ZnCl_2$ (0.136 g, 1.0 mmol), TeO_2 (0.160 g, 1.0 mmol) and $(NH_4)H_2PO_4$ (0.445 g, 3.0 mmol) were loaded into a Teflon-lined stainless-steel autoclave containing 3 mL of deionized water without stirring, followed by heating at 190 ℃ for 7 days, and then cooled down to room temperature naturally.

The resulting solid products were washed with deionized water in the ultrasonic machine for several times and then dried in air. Light green prism crystals of $Ni_2ZnTe^{IV}{}_2O_2(PO_4)_2(OH)_4$ (Fig. 1) were obtained in 90% yields based on Te mass. The presence of Ni, Zn, Te and P has been confirmed by EDX results with a molar ratio of Ni:Zn:Te:P ≈ 2:1:2:2. The experimental PXRD pattern shown in Fig. 2 agrees well with the calculated one based on single crystal data.

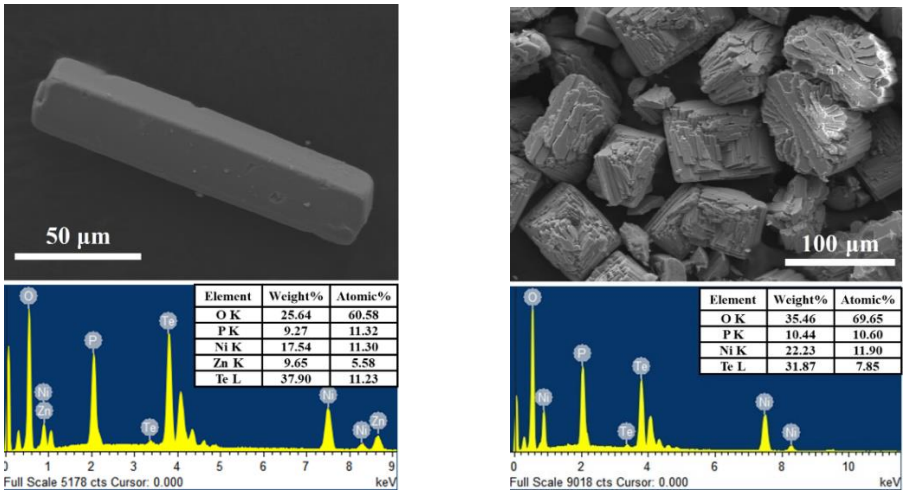

(a) **(b)**

Fig. 1. SEM images and EDX results of (a) $Ni_2ZnTe^{IV}{}_2O_2(PO_4)_2(OH)_4$ single crystal and (b) $Ni_3Te^{IV}{}_2O_2(PO_4)_2(OH)_4$

From the perspective of nonlinear optical crystals, we hope to get zinc tellurite phosphate in which the Zn^{2+} ions have large band gaps for optical transmission. The attempt to get unitary zinc tellurite phosphate was failed. However, by only adding a mixture of $NiCl_2$ $6H_2O$ (0.238 g, 1.0 mmol), TeO_2 (0.160 g, 1.0 mmol) and $(NH_4)H_2PO_4$ (0.445 g, 3.0 mmol) but removing $ZnCl_2$ from reactants, we can get a new unitary nickel tellurite phosphate $Ni_3Te^{IV}{}_2O_2(PO_4)_2(OH)_4$ isostructural to $Ni_2ZnTe^{IV}{}_2O_2(PO_4)_2(OH)_4$ confirmed by PXRD (Figs. 2 and 3) and EDX (Fig. 1b) results. However, it is difficult to get single crystals to determine the single-crystal structure of this nickel tellurite phosphate, since only bundles of crystals were obtained due to its uncontrollable crystallization behavior under current reaction conditions. Therefore, herein we only report the single crystal structure of $Ni_2ZnTe^{IV}{}_2O_2(PO_4)_2(OH)_4$.

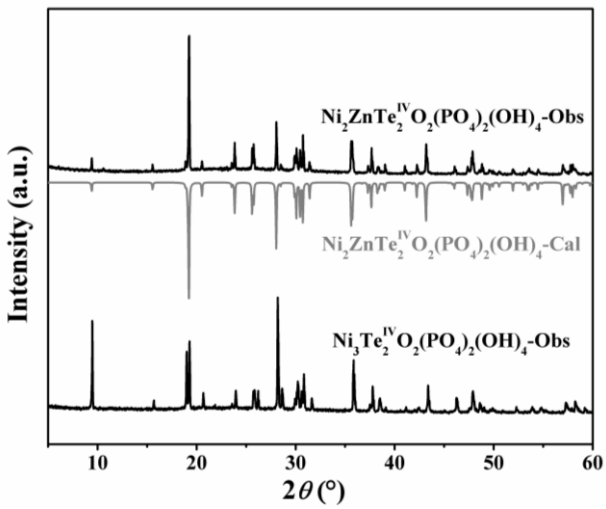

Fig. 2. Observed and calculated PXRD patterns of $Ni_2ZnTe^{IV}_2O_2(PO_4)_2(OH)_4$ together with the observed PXRD pattern of $Ni_3Te^{IV}_2O_2(PO_4)_2(OH)_4$

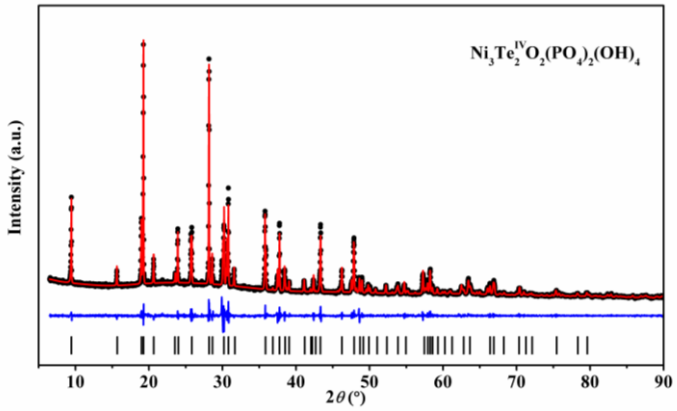

Fig. 3. Experimental (black dot) and calculated (red line) X-ray diffraction patterns of $Ni_3Te^{IV}_2O_2(PO_4)_2(OH)_4$. The difference profile (blue) and background (black) from Rietveld refinement (a = 19.2500(15) Å, b = 5.9352(6) Å, c = 4.7625(4) Å, β = 103.853(8)°, V = 528.31(2) Å^3, Z = 2, R_p = 4.121, R_{wp} = 6.177). The Bragg positions are indicated by the vertical bars below the patterns

2. 2 Characterization methods

Powder X-ray diffraction (PXRD) Powder X-ray diffraction data were collected on a Bruker D8 Advance powder X-ray diffractometer with Cu$K\alpha$ radiation (λ = 1.5418 Å, Ni filter, 40 kV and 40 mA).

Scanning electron microscopy/energy-dispersive analysis by X-ray (SEM/EDX) The crystal morphologies and element contents were investigated by utilizing a field-emission scanning electron microscopy (FE-SEM) system (Hitachi SU70) that was equipped with an energy-dispersive X-ray spectrometry device.

Infrared spectroscopy The infrared spectrum in the range of 400～4000 cm^{-1} was recorded on a Nicolet iS10 FT-IR spectrometer at room temperature.

Thermal analysis Thermal analyses were performed on a SDT Q600 thermogravimetric/differential scanning calorimetry (TG/DSC) instrument under conditions ranging from room temperature to 800 ℃ at a heating rate of 10 ℃ min^{-1} in a N_2 gas flow of 100 mL min^{-1}.

UV-vis-NIR diffuse reflectance spectroscopy The diffuse reflectance spectra were performed on a Varian Cary 5000 UV-Vis-NIR scan spectrometer, using $BaSO_4$ as the standard in the spectral range of 200～800 nm at room temperature.

Magnetic properties The magnetic susceptibilities were measured in gelatin capsules at a magnetic field of 1000 Oe using a Quantum Design MPMS XL-7 SQUID magnetometer in the temperature range of 2～300 K.

2. 3 Structure determination

A suitable single crystal (0.12mm × 0.03mm × 0.03mm) of $Ni_2ZnTe^{IV}_2O_2(PO_4)_2(OH)_4$ for single-crystal X-ray diffraction analysis has been selected under a binocular optical microscope, and further checked via its transparency and extinction under a polarized microscope. The data were

collected on an Oxford Gemini S Ultra diffractometer with Mo$K\alpha$ radiation (λ = 0.71073 Å, 50 kV and 40 mA) at 193(2) K. In the range of $3.58 \leqslant \theta \leqslant 28.26$°, a total number of 1730 reflections were collected and 664 were independent with R_{int} = 0.0355, of which 639 were observed with $I > 2\sigma(I)$. Multi-scan absorption correction has been performed. The crystal structure was solved by direct methods and refined by full-matrix least-squares technique using the SHELX programs[28] included in the WinGX package[29], and further checked for missing symmetry elements by using PLATON[30]. The atomic positions of Te, Ni, Zn, P and some coordinated O atoms were determined by direct methods. The rest O atom sites were located from difference Fourier maps. The bond valence sum calculations showing a low value of 1.63 for O(1) and 1.26 for O(2) indicate that the O(2) is a donor while the O(1) is an acceptor of hydroxyl group. However, no suitable position in difference Fourier maps could be located as H site. Hence, the H atoms were determined from theoretical calculation according to the empirical O−H distances 0.82(2) Å and the hydrogen bond requirement between O(1) and O(2) atoms. Meanwhile, the displacement parameters of H2 were constrained to be 0.05 e·Å^{-3}. The final full-matrix least-squares refinement converged to R = 0.0369 and wR = 0.1086 for 639 observed reflections with $I > 2\sigma(I)$, S = 1.103, D_c = 4.517 g cm^{-3}, μ(Mo$K\alpha$) = 11.434 mm^{-1} and F(000) = 672. The largest diffraction peak and hole are 1.49 and −1.91 e·Å^{-3}, respectively. The chemical formula was defined to be $Ni_2ZnTe^{IV}_2O_2(PO_4)_2(OH)_4$. The selected bond lengths and bond angles and the hydrogen bond lengths and bond angles of $Ni_2ZnTe^{IV}_2O_2(PO_4)_2(OH)_4$ are given in Tables 1 and 2, respectively.

Table 1. Selected Bond Lengths (Å) and Bond Angles (°) of $Ni_2ZnTe^{IV}_2O_2(PO_4)_2(OH)_4$

Bond	Dist.	Bond	Dist.	Bond	Dist.
Te(1)–O(5)	1.864(7)	Ni(1)–O(4)	2.074(5)	Zn(1)–O(2)^{vii}	2.104(5)
Te(1)–O(2)^{i}	2.003(5)	Ni(1)–O(5)^{ii}	2.114(5)	P(1)–O(3)	1.523(7)
Te(1)–O(2)	2.003(5)	Ni(1)–O(5)	2.114(5)	P(1)–O(1)	1.532(7)
Te(1)–O(4)	2.314(5)	Zn(1)–O(1)	2.060(6)	P(1)–O(4)^{viii}	1.544(5)
Te(1)–O(4)^{i}	2.314(5)	Zn(1)–O(1)^{iii}	2.060(6)	P(1)–O(4)^{ix}	1.544(5)
Ni(1)–O(3)^{ii}	2.045(5)	Zn(1)–O(2)^{iv}	2.104(5)	O(2)–H(2)	0.821(5)
Ni(1)–O(3)	2.045(5)	Zn(1)–O(2)^{v}	2.104(5)		
Ni(1)–O(4)^{ii}	2.074(5)	Zn(1)–O(2)^{vi}	2.104(5)		
Angle	(°)	Angle	(°)	Angle	(°)
O(5)–Te(1)–O(2)^{i}	92.7(2)	O(4)^{ii}–Ni(1)–O(5)^{ii}	78.3(2)	O(2)^{v}–Zn(1)–O(2)^{vii}	84.5(3)
O(5)–Te(1)–O(2)	92.7(2)	O(3)–Ni(1)–O(5)	95.8(2)	O(2)^{vi}–Zn(1)–O(2)^{vii}	180.0(3)
O(2)^{i}–Te(1)–O(2)	90.9(3)	O(3)^{ii}–Ni(1)–O(5)	84.2(2)	O(3)–P(1)–O(1)	108.7(4)
O(5)–Te(1)–O(4)	77.71(18)	O(4)–Ni(1)–O(5)	78.3(2)	O(3)–P(1)–O(4)^{viii}	110.0(2)
O(2)^{i}–Te(1)–O(4)	85.30(19)	O(4)^{ii}–Ni(1)–O(5)	101.7(2)	O(1)–P(1)–O(4)^{viii}	109.6(2)
O(2)–Te(1)–O(4)	169.51(19)	O(5)^{ii}–Ni(1)–O(5)	180.0	O(3)–P(1)–O(4)^{ix}	110.0(2)
O(5)–Te(1)–O(4)^{i}	77.71(18)	O(1)^{iii}–Zn(1)–O(1)	180.0	O(1)–P(1)–O(4)^{ix}	109.6(2)
O(2)^{i}–Te(1)–O(4)^{i}	169.51(19)	O(1)^{iii}–Zn(1)–O(2)^{iv}	92.65(19)	O(4)^{viii}–P(1)–O(4)^{ix}	108.8(4)
O(2)–Te(1)–O(4)^{i}	85.30(19)	O(1)–Zn(1)–O(2)^{iv}	87.35(19)	P(1)–O(1)–Zn(1)	128.1(4)
O(4)–Te(1)–O(4)^{i}	96.7(2)	O(1)^{iii}–Zn(1)–O(2)^{v}	87.35(19)	Te(1)–O(2)–Zn(1)^{x}	122.6(2)
O(3)–Ni(1)–O(3)^{ii}	180.0	O(1)–Zn(1)–O(2)^{v}	92.65(19)	P(1)–O(3)–Ni(1)^{xi}	130.89(18)
O(3)–Ni(1)–O(4)	90.3(2)	O(2)^{iv}–Zn(1)–O(2)^{v}	180.0(4)	P(1)–O(3)–Ni(1)	130.89(18)
O(3)^{ii}–Ni(1)–O(4)	89.7(2)	O(1)^{iii}–Zn(1)–O(2)^{vi}	87.35(19)	Ni(1)^{xi}–O(3)–Ni(1)	93.8(3)
O(3)–Ni(1)–O(4)^{ii}	89.7(2)	O(1)–Zn(1)–O(2)^{vi}	92.65(19)	P(1)^{xii}–O(4)–Ni(1)	131.2(3)
O(3)^{ii}–Ni(1)–O(4)^{ii}	90.3(2)	O(2)^{iv}–Zn(1)–O(2)^{vi}	84.5(3)	P(1)^{xii}–O(4)–Te(1)	125.8(3)
O(4)–Ni(1)–O(4)^{ii}	180.0	O(2)^{v}–Zn(1)–O(2)^{vi}	95.5(3)	Ni(1)–O(4)–Te(1)	95.04(18)
O(3)–Ni(1)–O(5)^{ii}	84.2(2)	O(1)^{iii}–Zn(1)–O(2)^{vii}	92.65(19)	Te(1)–O(5)–Ni(1)	108.9(2)
O(3)^{ii}–Ni(1)–O(5)^{ii}	95.8(2)	O(1)–Zn(1)–O(2)^{vii}	87.35(19)	Te(1)–O(5)–Ni(1)^{xiii}	108.9(2)
O(4)–Ni(1)–O(5)^{ii}	101.7(2)	O(2)^{iv}–Zn(1)–O(2)^{vii}	95.5(3)	Ni(1)–O(5)–Ni(1)^{xiii}	89.8(3)

Symmetry codes: (i) x, $-y+1$, z; (ii) $-x+1/2$, $-y+1/2$, $-z+1$; (iii) $-x+1$, $-y$, $-z$; (iv) $-x+1$, $-y+1$, $-z+1$; (v) x, $y-1$, $z-1$; (vi) x, $-y+1$, $z-1$; (vii) $-x+1$, $y-1$, $-z+1$; (viii) x, $-y$, $z-1$; (ix) x, y, $z-1$; (x) x, $y+1$, $z+1$; (xi) $-x+1/2$, $y-1/2$, $-z+1$; (xii) x, y, $z+1$; (xiii) $-x+1/2$, $y+1/2$, $-z+1$

Table 2. Hydrogen Bond Lengths (Å) and Bond Angles (°) of $Ni_2ZnTe^{IV}_2O_2(PO_4)_2(OH)_4$

D–H···A	d(D–H)	d(H···A)	d(D···A)	∠DHA
O(2)–H(2)···O(1)^{xiv}	0.82	2.00	2.819(8)	180

Symmetry code: (xiv) *x*, *y*+1, *z*

3 RESULTS AND DISCUSSION

3. 1 Crystal structure description

Both $Ni_3Te^{IV}_2O_2(PO_4)_2(OH)_4$ and $Ni_2ZnTe^{IV}_2O_2(PO_4)_2(OH)_4$ are new tellurite phosphates crystallizing in the monoclinic space group *C*2/*m* (No. 12) and isostructural to $Co_3Te_2O_2(PO_4)_2(OH)_4$[21]. Therefore, in the crystal structure of $Ni_3Te^{IV}_2O_2(PO_4)_2(OH)_4$, Ni atoms have two positions Ni(1) and Ni(2) according to the structure of $Co_3Te_2O_2(PO_4)_2(OH)_4$[21], while in $Ni_2ZnTe^{IV}_2O_2(PO_4)_2(OH)_4$, the original position of Ni(2) is completely replaced by Zn(1), which is confirmed by the results of single-crystal structure refinement and magnetic properties.

For $Ni_2ZnTe^{IV}_2O_2(PO_4)_2(OH)_4$, there is one unique site each for Te, Ni, Zn and P atoms, and five for O atoms in the asymmetric unit. The Te(1) atom, sited at the special position 4*i* (*m*), is five-coordinated to three O atoms and two OH groups to form a tetragonal pyramidal $TeO_3(OH)_2$. The Ni(1) atom (at an inversion center 4*f* (-1)) is in an octahedral coordination environment coordinated to six O atoms, resulting in a distorted NiO_6 octahedron. The Zn(1) atom occupied the special position of 2*b* (2/*m*) is six-coordinated to four OH groups at the equatorial plane and two O atoms at the apexes to form a compressed octahedral $ZnO_2(OH)_4$. The P(1) atom also sites at a special position 4*i* (*m*) which is four-coordinated to O atoms to form a regular PO_4 tetrahedron. The bond lengths of Te−O, Ni−O, Zn−O and P−O fall in the ranges of 1.864(7)～2.314(5), 2.045(5)～2.114(5), 2.060(6)～2.104(5) and 1.523(7)～1.544(5) Å, respectively. Meanwhile, the bond angles of O–Te–O, O–Ni–O, O–Zn–O and O–P–O vary from 77.71(18) to 169.51(19)°, 78.3(2) to 180.0°, 84.5(3) to 180.0°, and 108.7(4) to 110.0(2)°, respectively. These values are consistent with those related compounds reported previously[8, 16, 31]. The bond valence sum calculations[32] results on $Ni_2ZnTe^{IV}_2O_2(PO_4)_2(OH)_4$ are given in Table 3, revealing 1.92 Å for Ni(1), 2.12 Å for Zn(1), 4.00 Å for Te(1) and 4.98 Å for P(1) respectively, which are in their expected values[8, 16, 31].

Table 3. Bond Valence Sum Calculations of the Atoms in $Ni_2ZnTe^{IV}_2O_2(PO_4)_2(OH)_4$

Atom	Ni(1)	Zn(1)	Te(1)	P(1)	BVS
O(1)	-	+0.38 (+0.38×2)	-	+1.25 (+1.25)	1.63
O(2)	-	+0.34 (+0.34×4)	+0.92 (+0.92×2)	-	1.26
O(3)	+0.35×2 (+0.35×2)*	-		+1.29 (+1.29)	1.99
O(4)	+0.32 (+0.32×2)	-	+0.40 (+0.40×2)	+1.22 (+1.22×2)	1.94
O(5)	+0.29×2 (+0.29×2)	-	+1.36 (+1.36)	-	1.94
BVS	1.92	2.12	4.00	4.98	-

*(+*n*) is for the BVS of line atoms and +*n* for the BVS of column atoms.

As is shown in Fig. 4, each NiO_6 octahedron connects the neighboring counterparts via trans-edge-sharing to form an infinite linear chain along the *b*-axis (Fig. 4a). Neighboring linear chains are intra- and inter-connected by PO_4 tetrahedra via vertex-sharing, forming 4-membered rings (4-MR) and 3-membered rings (3-MR) (Fig. 4b) which result in the $[Ni_2O_2(PO_4)_2]^{6-}$ layers parallel to the *bc*-plane (Fig. 4b, 4c, 4e). Each $ZnO_2(OH)_4$ octahedron shares four equatorial OH groups each with a $TeO_3(OH)_2$ tetragonal pyramid forming a four-member ring (4-MR) single chain $[ZnTe_2O_2(OH)_4]^{2+}$ running along the *b*-axis (Fig. 4d). Finally, the $[Ni_2O_2(PO_4)_2]^{6-}$ layers are interconnected by $[ZnTe_2O_2(OH)_4]^{2+}$ single chains via vertex-sharing to form a three-dimensional framework structure (Fig. 4e & 4f). In a unit cell, the neighboring $[Ni_2O_2(PO_4)_2]^{6-}$ layers are antiparallelly arranged, leading to the extra-large *a*-axis (*a* =

19.3247(10) Å). Alternately, the crystal structure can also be looked as isolated $ZnO_2(OH)_4$ octahedra at the middle points of [100] and [010] edges linked to the trans-edge sharing $[NiO_6]$ linear chains at (1/4, *y*, 1/2) and (3/4, *y*, 1/2) via isolated $[PO_4]$ tetrahedra and $TeO_3(OH)_2$ tetragonal pyramids to form a three-dimensional crystal structure (Fig. 4e & 4f).

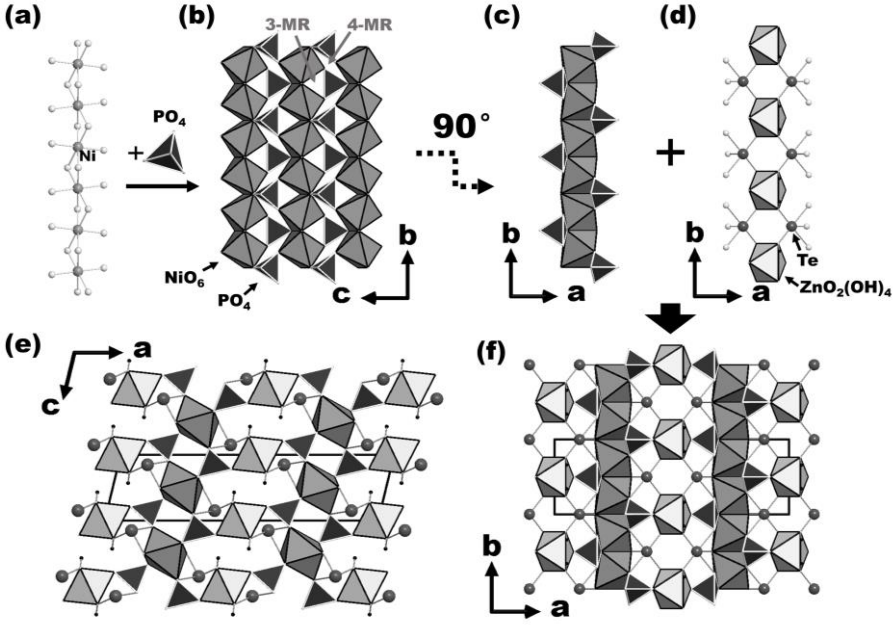

Fig. 4. Crystal structure of $Ni_2ZnTe^{IV}{}_2O_2(PO_4)_2(OH)_4$. (a) 1*D* linear NiO_6 octahedral chain running along the *b*-axis; (b) $[Ni_2O_2(PO_4)_2]^{6-}$ layer paralleling to the *bc*-plane built from linear NiO_6 octahedral chains intra- and inter-connected by PO_4 tetrahedra via vertex sharing; (c) $[Ni_2O_2(PO_4)_2]^{6-}$ layer viewed along the *c*-axis; (d) $[ZnTe_2O_2(OH)_4]^{2+}$ single chain running along the *b*-axis built from $ZnO_2(OH)_4$ octahedra and $TeO_3(OH)_2$ tetragonal pyramids; (e) Crystal structure viewed along the *b*-axis; (f) Crystal structure viewed along the *c*-axis. NiO_6 octahedra, dark-gray; $ZnO_2(OH)_4$ octahedra, light-gray; PO_4 tetrahedra, black; Te atoms, dark-gray balls; Ni atoms, medium-gray balls; O atoms, light-gray balls; H atoms, small black balls

It is needed to note that, due to the existence of SCALP, the Te^{4+} located at mirror plane (*y* = 0 or 1/2) forms an acentric tetragonal pyramid $TeO_3(OH)_2$, which has inherent dipole moment. The calculated value of $TeO_3(OH)_2$ dipole moment is 8.39 Debyes according to the method described by Maggard et al.[33]. However, as shown in Fig. 5, $TeO_3(OH)_2$ tetragonal pyramids do not connect to each other, and arrange in a centrosymmetric (2/*m*) correlation in the unit cell, i.e. the dipole moment directions are arranged in an antiparallel manner. As a result, the adjacent dipole moments offset each other, which leads to the formation of a centrosymmetric crystal structure. The isolated acentric $TeO_3(OH)_2$ units are easily affected by other structural units and aligned in a centrosymmetric arrangement. We suppose that the polymerization of acentric units TeO_x may reserve their non-centrosymmetric characteristics and that could be an efficient route to design non-centrosymmetric crystal structure.

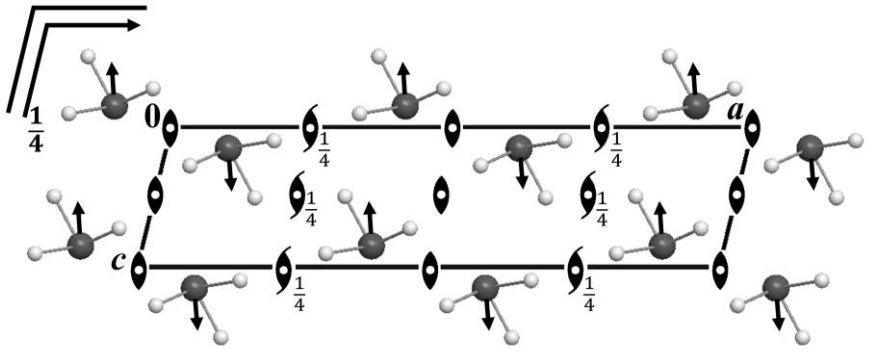

Fig. 5. Site arrangement of $TeO_3(OH)_2$ in the unit cell with symmetry graphical symbol, where black arrows represent the dipole moments. Other atoms are omitted for clarity

3. 2 Infrared spectroscopy

The infrared spectra (Fig. 6) of $Ni_2ZnTe^{IV}{}_2O_2(PO_4)_2(OH)_4$ and $Ni_3Te^{IV}{}_2O_2(PO_4)_2(OH)_4$ reveals that both compounds show similar absorption bands and consist of P−O, Te−O, Te−O−P and O−H vibrations. In the following assignments, two absorption band values (value 1/value 2) belong to $Ni_2ZnTe^{IV}{}_2O_2(PO_4)_2(OH)_4$/$Ni_3Te^{IV}{}_2O_2(PO_4)_2(OH)_4$, respectively. The broad bands at around 3209/3205 cm^{-1} are assigned to the O−H stretching vibrations. The absorption bands at 1047～975/1047～976 cm^{-1} can be assigned to the P−O stretching vibrations whereas the bands at 725/719 cm^{-1} can be attributed to the Te−O stretching vibrations. The bands at 608/610 cm^{-1} can be assigned to the Te−O−P vibrations, whereas the bands at 538/540 and 447/449 cm^{-1} can be attributed to the P−O bending vibrations. The above band absorptions are similar with those in related compounds[16, 34], confirming the existence of OH, $TeO_3(OH)_2$ and PO_4 groups.

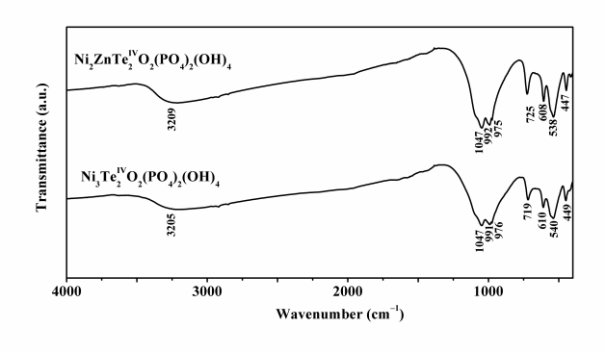

Fig. 6. Infrared spectra of $Ni_2ZnTe^{IV}{}_2O_2(PO_4)_2(OH)_4$ and $Ni_3Te^{IV}{}_2O_2(PO_4)_2(OH)_4$

3. 3 Thermal analysis

The thermal analysis results of $Ni_2ZnTe^{IV}{}_2O_2(PO_4)_2(OH)_4$ and $Ni_3Te^{IV}{}_2O_2(PO_4)_2(OH)_4$ are shown in Fig. 7. TG curves of two compounds show significant weight loss in the temperature range of 300 ～ 600 ℃. For $Ni_2ZnTe^{IV}{}_2O_2(PO_4)_2(OH)_4$, the observed weight loss is 5.68 wt%, which agrees with the calculated value of 4.94 wt% for removing OH groups (2×H_2O per formula unit). For $Ni_3Te^{IV}{}_2O_2(PO_4)_2(OH)_4$, the observed weight loss is 6.32 wt%, also consistent with the calculated value of 4.99 wt% for removing OH groups. The relatively large observed weight loss of both compounds could be attributed to the condensation of OH groups accompanied with the evaporation of TeO_2. The results further confirm the existence of OH groups.

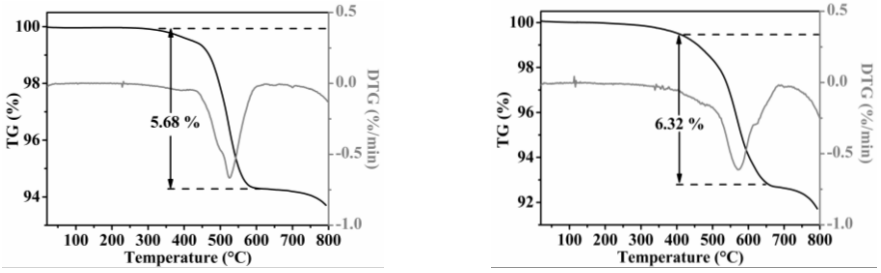

Fig. 7. TG-DTG curves of $Ni_2ZnTe^{IV}{}_2O_2(PO_4)_2(OH)_4$ (a) and $Ni_3Te^{IV}{}_2O_2(PO_4)_2(OH)_4$ (b)

3. 4 UV-Vis-NIR diffuse reflectance spectroscopy

The UV-Vis-NIR diffuse reflectance spectra of $Ni_2ZnTe^{IV}{}_2O_2(PO_4)_2(OH)_4$ and $Ni_3Te^{IV}{}_2O_2(PO_4)_2(OH)_4$ (Fig. 8) show that the transmission ranges are limited by nickel element. They have wide absorption ranges in the UV and near infrared range together with a valley at around 400 nm. The highest reflectance peaks at 533 nm are consistent with the green color of the observed crystals for the title two compounds.

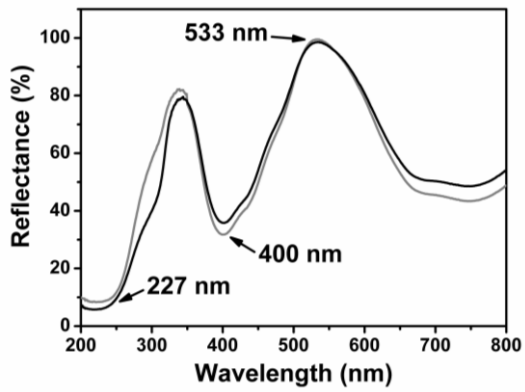

Fig. 8. UV-Vis-NIR diffuse reflectance spectra of $Ni_2ZnTe^{IV}{}_2O_2(PO_4)_2(OH)_4$ (black curve) and $Ni_3Te^{IV}{}_2O_2(PO_4)_2(OH)_4$ (gray curve)

3. 5 Magnetic properties

Fig. 9 shows the magnetic susceptibility (χ) and reciprocal susceptibility ($1/\chi$) curves of $Ni_3Te^{IV}{}_2O_2(PO_4)_2(OH)_4$ and $Ni_2ZnTe^{IV}{}_2O_2(PO_4)_2(OH)_4$ in the temperature range of 2～300 K.

For $Ni_3Te^{IV}{}_2O_2(PO_4)_2(OH)_4$, the Curie-Weiss law is observed between 30 and 250 K and gives the Weiss temperature θ = −22.6 K which indicates predominant antiferromagnetic spin-exchange interaction. The effective magnetic moment $\mu_{eff(Ni\text{-}atom)}$ = 3.31 μ_B indicates the existence of orbital coupling effect besides the interaction between electron spins only ($\mu_{spin\text{-}only}$ = 2.83 μ_B). Its magnetic characteristics are similar to those of $Co_3Te_2O_2(PO_4)_2(OH)_4$[21]. Two maxima are observed at low temperature. The maximum at 20 K is most likely due to a two-dimensional antiferromagnetic ordering of linear $[Ni(1)O_6]$ chains coupled by interchain interaction via $[PO_4]$ groups in the $[Ni_2O_2(PO_4)_2]^{6-}$ layer (Fig. 4b). The second maximum at around 5 K is probably due to the Ni(2) entities via super-super exchange involving $[PO_4]$ and $[TeO_3(OH)_2]$ groups.

For $Ni_2ZnTe^{IV}{}_2O_2(PO_4)_2(OH)_4$, from 30 to 250 K its magnetic susceptibility follows the Curie-Weiss law, with a Weiss temperature θ = −10.9 K and effective magnetic moment of $\mu_{eff(Ni\text{-}atom)}$ = 3.11 μ_B. Only one maximum is observed at low temperature. Obviously, the magnetic properties of two compounds are quite different, indicating magnetic structure difference between them.

The magnetic species in both compounds are Ni atoms. Generally, from the perspective of crystallography, Ni and Zn may co-occupy in one site due to their similar radius and coordination environments. If this is the case for $Ni_2ZnTe^{IV}{}_2O_2(PO_4)_2(OH)_4$, the magnetic ordering at low temperature of $Ni_2ZnTe^{IV}{}_2O_2(PO_4)_2(OH)_4$ should be similar to that of $Ni_3Te^{IV}{}_2O_2(PO_4)_2(OH)_4$. However, $Ni_2ZnTe^{IV}{}_2O_2(PO_4)_2(OH)_4$ takes another magnetic susceptibility compared to $Ni_3Te^{IV}{}_2O_2(PO_4)_2(OH)_4$. Furthermore, counting on the molar ratio of Ni:Zn = 2:1 according to EDX results, Zn sitting at the special position 2*b* of Ni(2) while Ni locating at the special position 4*f* of Ni(1) just fits the molar ratio requirement that could lead to different magnetic structures compared with $Ni_3Te^{IV}{}_2O_2(PO_4)_2(OH)_4$. Therefore, Zn(1) does not partially replace both Ni(1) and Ni(2) positions but completely substitute the Ni(2) position. The results further confirm the single crystal refinement results.

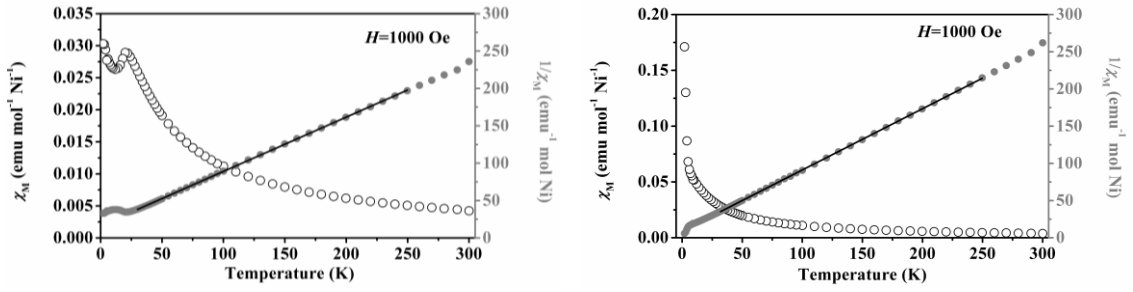

Fig. 9. Temperature dependence of magnetic susceptibility (χ) and the corresponding reciprocal susceptibility ($1/\chi$) for (a) $Ni_3Te^{IV}{}_2O_2(PO_4)_2(OH)_4$ and (b) $Ni_2ZnTe^{IV}{}_2O_2(PO_4)_2(OH)_4$. Hollow circle, magnetic susceptibility; solid gray circle, the reciprocal of susceptibility; black line, the fitting line

4 CONCLUSION

In summary, we have successfully synthesized two isostructural tellurite phosphates $Ni_2M^{II}Te^{IV}{}_2O_2(PO_4)_2(OH)_4$ (M^{II} = Ni, Zn) via hydrothermal method. The crystal structure of $Ni_2M^{II}Te^{IV}{}_2O_2(PO_4)_2(OH)_4$ (M^{II} = Ni, Zn) features a 3*D* framework composed of $[Ni_2O_2(PO_4)_2]^{6-}$ layers interconnected by $[MTe_2O_2(OH)_4]^{2+}$ single chains. Different magnetic susceptibility results at low temperature of the two title compounds confirm that Zn(1) completely occupies the Ni(2) position but not partially substitutes both Ni(1) and Ni(2) position atoms. The acentric $TeO_3(OH)_2$ tetragonal pyramids are aligned in an antiparallel manner, resulting in the crystallization of centrosymmetric (*C*2/*m*) crystal structure for the title compound. The investigation of the origin of centrosymmetric crystal structure with strong dipole moment units provides deeper understanding for future rational design of non-centrosymmetric crystal structure. To the best of our knowledge, $Ni_2ZnTe^{IV}{}_2O_2(PO_4)_2(OH)_4$ is the first mix transition metal tellurite phosphate up to now.

REFERENCES

(1) Halasyamani, P. S.; Poeppelmeier, K. R. Noncentrosymmetric oxides. *Chem. Mater.* **1998**, 10, 2753–2769.

(2) Guesdon, A.; Raveau, B. A series of Mo(VI) monophosphates involving the lone pair cation Te(IV): $A_2TeMo_2O_6(PO_4)_2$ (*A* = K, Rb, Tl, Cs). *Chem. Mater.* **2000**, 12, 2239–2243.

(3) Halasyamani, P. S. Asymmetric cation coordination in oxide materials: influence of lone-pair cations on the intra-octahedral distortion in d^0 transition metals. *Chem. Mater.* **2004**, 16, 3586–3592.

(4) Mao, J. G.; Jiang, H. L.; Kong, F. Structures and properties of functional metal selenites and tellurites. *Inorg. Chem.* **2008**, 47, 8498–8510.

(5) Ok, K. M.; Orzechowski, J.; Halasyamani, P. S. Synthesis, structure, and characterization of two new layered mixed-metal phosphates, $BaTeMO_4(PO_4)$ (*M* = Nb^{5+} or Ta^{5+}). *Inorg. Chem.* **2004**, 43, 964–968.

(6) Ok, K. M.; Halasyamani, P. S. Asymmetric cationic coordination environments in new oxide materials: synthesis and characterization of $Pb_4Te_6M_{10}O_{41}$ (*M* = Nb^{5+} or Ta^{5+}). *Inorg. Chem.* **2004**, 43, 4248–4253.

(7) Kim, M. K.; Kim, S. H.; Chang, H. Y.; Halasyamani, P. S.; Ok, K. M. New noncentrosymmetric tellurite phosphate material: synthesis, characterization, and calculations of $Te_2O(PO_4)_2$. *Inorg. Chem.* **2010**, 49, 7028–7034.

(8) Tang, X. Y.; Mi, J. X.; Zhuang, R. C.; Wang, S. H.; Wu, S. F.; Pan, Y. M.; Huang, Y. X. Rational design and synthesis of a deep-ultraviolet nonlinear optical fluorinated orthophosphate: $BaZn(PO_4)F$. *Inorg. Chem.* **2019**, 58, 4508–4514.

(9) Tang, R. L.; Hu, C. L.; Wu, B. L.; Fang, Z.; Chen, Y.; Mao, J. G. $Cs_2Bi_2O(Ge_2O_7)$ (CBGO): a larger SHG effect induced by synergistic polarizations of BiO_5 polyhedra and GeO_4 tetrahedra. *Angew. Chem. Int. Ed.* **2019**, 58, 15358–15361.

(10) Wen, M.; Hu, C.; Wu, H. P.; Yang, Z. H.; Yu, H. H.; Pan, S. L. Three non-centrosymmetric bismuth phosphates, $Li_2ABi(PO_4)_2$ (*A* = K, Rb, and Cs): effects of cations on the crystal structure and SHG response. *Inorg. Chem. Front.* **2020**, 7, 3364–3370.

(11) Ma, Y. X.; Gong, Y. P.; Hu, C. L.; Kong, F.; Mao, J. G. $BiGa(SeO_3)_3$: a phase matchable SHG material achieved by cation substitution. *Inorg. Chem.* **2020**, 59, 7852–7859.

(12) Wen, M.; Hu, C.; Yang, Z. H.; Wu, X. H.; Pan, S. L. $K_2TeP_2O_8$: a new telluro-phosphate with a pentagonal Te-P-O layer structure. *Dalton Trans.* **2018**, 47, 9453–9458.

(13) Pearson, R. G. The second-order Jahn-Teller effect. *J. Mol. Struct. Theochem.* **1983**, 12, 25–34.

(14) Ok, K. M.; Halasyamani, P. S. Mixed-metal tellurites: synthesis, structure, and characterization of $Na_{1.4}Nb_3Te_{4.9}O_{18}$ and $NaNb_3Te_4O_{16}$. *Inorg. Chem.* **2005**, 44, 3919–3925.

(15) Christy, A. G.; Mills, S. J.; Kampf, A. R. A review of the structural architecture of tellurium oxycompounds. *Mineral. Mag.* **2016**, 80, 415–545.

(16) Li, L.; Zhuang, R. C.; Mi, J. X.; Huang, Y. X. A new modification of tellurite phosphate β-$Te_3O_3(PO_4)_2$. *Chin. J. Struct. Chem.* **2018**, 37, 1417–1425.

(17) Kim, J. H.; Halasyamani, P. S. A rare multi-coordinate tellurite, $NH_4ATe_4O_9$ $2H_2O$ (*A* = Rb or Cs): the occurrence of TeO_3, TeO_4, and TeO_5 polyhedra in the same material. *J. Solid State Chem.* **2008**, 181, 2108–2112.

(18) Mayer, H.; Weil, M. Synthesis and crystal structure of $Te_3O_3(PO_4)_2$, a compound with 5-fold coordinate tellurium (IV). *Z. Anorg. Allg. Chem.* **2003**, 629, 1068–1072.

(19) Ok, K. M.; Halasyamani, P. S. Synthesis, structure, and characterization of a new one-dimensional tellurite phosphate, $Ba_2TeO(PO_4)_2$. *J. Solid State Chem.* **2006**, 179, 1345–1350.

(20) Schmidt, P.; Dallmann, H.; Kadner, G.; Krug, J.; Philipp, F.; Teske, K. The thermochemical behaviour of $Te_8O_{10}(PO_4)_4$ and its use for phosphide

telluride synthesis. *Z. Anorg. Allg. Chem.* **2009**, 635, 2153–2161.

(21) Zimmermann, I.; Kremer, R. K.; Johnsson, M. Synthesis, crystal structure and magnetic properties of the open framework compound $Co_3Te_2O_2(PO_4)_2(OH)_4$. *J. Solid State Chem.* **2011**, 184, 3080–3084.

(22) Xia, M. J.; Li, R. K. Structural variety in zinc telluro-phosphates: syntheses, crystal structures and characterizations of $Sr_2Zn_3Te_2P_2O_{14}$, $Pb_2Zn_3Te_2P_2O_{14}$ and $Ba_2Zn_2TeP_2O_{11}$. *Dalton Trans.* **2016**, 45, 7492–7499.

(23) Shen, Y. G.; Zhao, S. G.; Luo, J. H. Study on nonlinear optical properties of Te_2HPO_7 crystal. *J. Synth. Cryst.* **2016**, 45, 1487–1491.

(24) Li, Z.; Zhang, S. Z.; Yin, W. L.; Lin, Z. S.; Yao, J. Y.; Wu, Y. C. $Na_3Ca_4(TeO_3)(PO_4)_3$: a new noncentrosymmetric tellurite phosphate with fascinating multimember-ring architectures and intriguing nonlinear optical performance. *Dalton Trans.* **2018**, 47, 17198–17201.

(25) Alcock, N. W.; Harrision, W. D. Refinement of the structure of tellurium phosphate $Te_2O_3HPO_4$. *Acta Crystallogr. Sect. B: Struct. Sci.* **1982**, 38, 1809–1811.

(26) Xia, M. J.; Shen, S. P.; Lu, J.; Sun, Y.; Li, R. K. $Ba_2Cu_2Te_2P_2O_{13}$: a new telluro-phosphate with S = 1/2 heisenberg chain. *J. Solid State Chem.* **2015**, 230, 75–79.

(27) Zhao, M.; Sun, Y. J.; Wu, Y. D.; Mei, D. J.; Wen, S. G.; Doert, T. $NaTePO_5$, $SrTeP_2O_8$ and $Ba_2TeP_2O_9$: three tellurite-phosphates with large birefringence. *J. Alloys Compd.* **2021**, 854, 157243–11.

(28) Sheldrick, G. Crystal structure refinement with SHELXL. *Acta Crystallogr. Sect. C: Cryst. Struct. Commun.* **2015**, 71, 3–8.

(29) Farrugia, L. J. Wingx: suite for small-molecule single-crystal crystallography. *J. Appl. Crystallogr.* **1999**, 32, 837–838.

(30) Spek, A. Single-crystal structure validation with the program PLATON. *J. Appl. Crystallogr.* **2003**, 36, 7–13.

(31) Liu, L. C.; Ren, W. J.; Huang, Y. X.; Pan, Y. M.; Mi, J. X. Canted antiferromagnetism in $KNi_3[PO_3(F,OH)]_2[PO_2(OH)_2]F_2$ with a stair-case kagome lattice. *J. Solid State Chem.* **2017**, 254, 160–165.

(32) Brese, N. E.; Okeeffe, M. Bond-valence parameters for solids. *Acta Crystallogr. Sect. B: Struct. Sci.* **1991**, 47, 192–197.

(33) Maggard, P. A.; Nault, T. S.; Stern, C. L.; Poeppelmeier, K. R. Alignment of acentric $MoO_3F_3^{3-}$ anions in a polar material: $(Ag_3MoO_3F_3)(Ag_3MoO_4)Cl$. *J. Solid State Chem.* **2003**, 175, 27–33.

(34) Yang, D.; Zhuang, R. C.; Mi, J. X.; Huang, Y. X. Two alkali metal germanophosphates $Na_3[Ge(OH)(PO_4)_2]\ 2H_2O$ and $Li_2Na[GeO(HPO_4)(PO_4)]$: crystal structures and thermal stability. *Chin. J. Struct. Chem.* **2021**, 40, 114–124.